Comparative analysis of non structural protein 1 of SARS-COV2 with SARS-COV1 and MERS-COV: An i*n silico* study

Ankur Chaudhuri

Department of Microbiology, West Bengal State University, Barasat, Kolkata - 700126, India

Abstract

The recently emerged SARS-COV2 caused a major pandemic of coronavirus disease (COVID-19). The main goal of this study is to elucidate the structural conformations of non structural protein 1(nsp1), prediction of epitope sites and identification of important residues for targeted therapy against COVID-19. In this study, molecular modelling coupled with molecular dynamics simulations were performed to analyse the conformational change of SARS-COV1, SARS-COV2 and MERS-COV at molecular level. Free energy landscape was constructed by using the first (PC1) and second (PC2) principle components. From the sequence alignment it was observed when compared to SERS-COV1 28 mutations are present in SERS-COV2 nsp1 protein. Several B-cell and T-cell epitopes were identified by immunoinformatics study. The ΔG values for SARS-COV1, SARS-COV2 and MERS-COV nsp1 proteins were 4.44, 5.82 and 6.15 kJ/mol respectively. SARS-COV2 nsp1 protein binds with the interface region of the palm and finger domain of POLA1 by using hydrogen bonds and salt bridges interactions. The present study provided a comprehensive structural model of nsp1 by threading process. The MD simulation parameters indicated that all three nsp1 proteins were stable during the simulation run. These findings can be used to develop therapeutics specific against COVID-19.

Key words: Non structural protein1, COVID-19, protein modelling, simulation, immunoinformatics, protein-protein docking

Author to correspondence: Ankur Chaudhuri (chaudhuriankur9@gmail.com)

1. Introduction

In December 2019, the first epidemic novel coronavirus (SARS-COV2) was identified in Wuhan city, China [1, 2]. Since the outbreak, WHO (World Health Organization) declared the COVID-19 as a pandemic on March 11, 2020 and posed a global health emergency. The causative agent of the COVID-19 disease is a severe acute respiratory syndrome coronavirus 2 (SARS-CoV-2). The worldwide number of coronavirus cases reached to 5,503,005 with a death toll of 346,768 as of May 25, 2020 [3]. Although it was first reported from China, the number of active cases in India, USA, Brazil, Russia, Spain, Italy, France, Germany, and UK have surpassed the cases identified in China (82,985). Almost all countries initiated social distancing and locked down precautions to avoid human to human transmission for till date no human vaccine is available in the market for COVID-19 treatment. Coronaviruses are enveloped, positive-sense, single-stranded RNA viruses (ssRNA+) belonging to the Coronaviridae family. COVID-19 is a member of beta coronaviruses, like the other human coronaviruses SARS-COV and MERS-COV [2,4]. There are seven strains of human CoVs, which include NL63, 229E, HKU1, OC43, Middle East respiratory syndrome (MERS-COV), severe acute respiratory syndrome (SARS-COV or SARS-COV1), and 2019-novel coronavirus (SARS-COV2), responsible for the infection of the respiratory tract. Among these seven strains, three strains are highly pathogenic (SARS-COV1, SARS-COV2 and MERS-COV) and are responsible for lower respiratory ailment like bronchiolitis, bronchitis, and pneumonia [5]. Sequence analysis of SARS-COV2 suggests that the genome size of this virus is 30kb and encodes structural and non-structural proteins like other CoVs. The two-thirds of the 5′ end of the CoV genome consists of two overlapping open reading frames (Orfs 1a and 1b) that encode non-structural proteins (nsps). The other one-third of the genome consists of ORFs that encodes structural proteins. Structural protein consists of S protein (Spike), E protein (Envelope), M protein (Membrane), and N protein (Nucleocapsid) [6, 7]. The Orf1a and Orf1b encodes a polyprotein which is cleaved into sixteen non-structural proteins (nsp1-16) that form the replicase / transcriptase complex (RTC) [8]. Alpha and beta CoVs consists of 16 nsps, while gamma and delta CoVs, lacking nsp1, consists of 15 nsps (nsp2-16) [9]. The amino acid sequences of nsp1 are highly divergent among CoVs [10]. It is among the least well-understood nsps, and other than in coronaviruses, no viral or cellular homologs are reported.

The nsp1 of SARS-COV inhibits host gene expression by blocking the translation process through interaction with 40S ribosomal subunit and degrades host mRNA via the recruitment of unidentified host nuclease(s) [11, 12]. SARS-CoV nsp1 inhibits the expression of the IFN genes and the host antiviral signaling pathway in the infected cells. The dysregulation of IFN genes is the key factor for inducing lethal pneumonia [13, 14]. MERS-CoV nsp1 also induced mRNA degradation and translational suppression. SARS-COV nsp1 also regulates the induction of cytokines and chemokine in human lung epithelial cells [15]. Thus, nsp1 is considered a major possible virulence factor for coronaviruses. SARS-COV2 nsp1 antagonizes interferon induction to suppress the host antiviral response. The inflammatory phenotype of SARS-COV and SARS-COV-2 pathology was also contributed by nsp1 protein [15]. The nsp1 protein of SARS-COV2 interacts with six proteins of the infected host cells. They are POLA1, POLA2, PRIM1, PRIM2, PKP2 and COLGALT1. Four of these host proteins (POLA1, POLA2, PRIM1 and PRIM2) form DNA polymerase alpha complexes. This events raise the possibility that the nsp1 protein of SARS-COV2 may interact to DNA polymerase alpha complex and change its functional activity to antagonise the innate immune system [8].

The main goal of this study is to propose a molecular model of the nsp1 protein and nsp1-POLA1 complex. The epitope sites of SARS-COV1, SARS-COV2 and MERS-COV nsp1 protein were identified by immunoinformatics process. Molecular dynamics simulation, principal component analysis (PCA), and Gibbs free energy landscape (FEL) were performed to assess the conformational changes of the SARS-COV1, SARS-COV2 and MERS-COV nsp1 protein. The mutated amino acids of SARS-COV2 nsp1 protein were reported by using multiple sequence alignment. The binding interactions of SARS-COV2 nsp1 protein and POLA1 were studied by implementing protein-protein docking procedure to identify the important interacting residues at the interface region. The epitope prediction and conformational analysis can be utilised in drug design and vaccine development process by targeting the virulence factor nsp1.

2. Materials and methods

2.1 Sequence retrieval

The protein sequences of nsp1 were retrieved from the curated NCBI database [16]. The accession number of the nsp1 of SARS-COV1, SARS-COV2 and MERS-COV are NP_828860.2, YP_009725297.1 and YP_009047213.1 respectively. The pairwise sequence identity between COVID-19 nsp1 protein and each of the other HCoV nsp1 proteins (SERS-COV1 and MERS-COV) was calculated using the BLASTp (basic local alignment tool) [17]. To check the conservation pattern, multiple sequence alignment (MSA) of all of the nsp1 sequences was performed using the Clustal Omega programme of the European Bioinformatics Institute (EMBL-EBI) [18].

2.2 Three dimensional structure prediction

The NMR structure of the non structural protein 1 (nsp1) of SERS-COV1 was identified by Almeida et al in 2007 and deposited in PDB as ID no. 2hsx/2gdt [19]. Currently no crystallographic structure of nsp1 of SARS-COV2 and MERS-COV is available in Protein Data Bank (PDB). So, in silico modelling study was employed to predict the three dimensional structure of nsp1 of SARS-COV2 and MERS-COV by using the I-TASSER web server [20]. I-TASSER (Iterative Threading ASSEmbly Refinement) is a bioinformatics approach to predict the structure and function of an unknown protein molecule. It first detects structural templates from the protein data bank (PDB) database by fold recognition or multiple threading approach LOMETS [21]. The full-length atomic models are constructed by iterative template-based fragment assembly simulations. The predicted protein models are constructed by continuous assembling of the aligned region with templates and initiating an *ab initio* folding for the unaligned regions based on replica exchange Monte Carlo simulation process. This simulation method generates an ensemble of several conformations which are further clustered on the basis of free energy. The lowest energy predicted structures are subjected to a refinement process resulting in a final three dimensional protein structural model. I-TASSER (as 'Zhang-Server') has regularly been the top ranked server for prediction of protein structure in recent community-wide CASP (Critical Assessment of Protein Structure Prediction) method experiments [22]. The modelled nsp1 proteins were optimised to avoid any stereochemical restraints by steepest descent energy minimization method. The stereochemical quality of the nsp1 proteins was validated by Ramachandran plot using PROCHECK [23, 24]. The models were further validated by ProSA [25], ProQ [26].

2.3 Active site prediction

The ligand binding residues of nsp1 of SARS-COV1, SARS-COV2 and MERS-COV were predicted by COACH meta server [27]. COACH generates complementary ligand binding sites of the target proteins by using two comparative processes, S-SITE and TM-SITE. These two methods recognize ligand-binding templates from the BioLiP database [28] by sequence profile comparisons and binding-specific substructure.

2.4 Prediction of T-cell (HLA class I and II) epitopes

The RANKPEP, sequence-based screening server was used to identify the T-cell epitopes [29] of the nsp1 protein of SARS-COV1, SARS-COV2 and MERS-COV. This server predicts the short peptide that binds to MHC molecules from protein sequences using the position-specific scoring matrix (PSSM). All the HLA class I alleles were selected for prediction of epitopes of HLA class I. For the prediction of epitopes of HLA class II, we selected some alleles such as DRB10101, DRB10301, DRB10401, DRB10701, DRB10801, DRB11101, DRB11301, and DRB11501 that cover HLA variability of over 95% of the human population worldwide [30].

2.5 B-cell epitopes (linear) identification

B-cell epitopes of the three nsp1 protein were predicted by using BepiPred and Kolaskar & Tongaonkar Antigenicity (http://www.iedb.org/) servers [31]. BepiPred for linear epitope prediction uses both amino acid propensity scales and hidden Markov model methods. The cut off score for linear B-cell epitopes prediction is 0.50. Kolaskar and Tongaonkar evaluate the protein for B cell epitopes using the physicochemical properties of the amino acids and their frequencies of occurrence in recognized B cell epitopes [32, 33].

2.6 Molecular dynamics simulation

Molecular dynamics simulations are used to predict the dynamic behaviour of the protein macromolecule at the atomic level. The nsp1 protein of SERS-COV1, SARS-COV2 and MERS-COV were subjected to MD simulation by using Gromacs v 2018.2 software suite [34] with OPLS-AA force field [35]. The three systems were solvated in a cubic box with SPC (simple

point charge) water model [36] by maintaining periodic boundary condition (PBC) through the simulation process. Sodium and chloride ions were added to neutralize the three systems. Each system was energy minimized using the steepest descent algorithm until the maximum force was found to be smaller than 1000.0 kJ/mol/nm. This was done to remove any steric clashes on the system. Each system was equilibrated with 100 ps isothermal-isochoric ensemble, NVT (constant number of particles, volume, and temperature) followed by 100 ps isothermal-isobaric ensemble NPT (constant number of particles, pressure, and temperature). The two types of ensemble of equilibration method stabilized the three systems at 300 K and 1 bar pressure. The Berendsen thermostat and Parrinello-Rahman were applied for temperature and pressure coupling method respectively [37]. Particle Mesh Ewald (PME) method [38] was used for the calculations of the long range electrostatic interactions and the cut off radii for Van der Waals and coulombic short-range interactions were set to 0.9 nm. The Linear Constraint Solver (LINCS) constraints algorithm was used to fix the lengths of the peptide bonds and angles [39]. All the three systems were subjected to MD simulations for 2000 ps.

2.7 Molecular dynamics simulation analysis

The MD simulations of three nsp1 proteins of SERS-COV1, SERS-COV2 and MERS-COV performed in this study were analyzed using various inbuilt scripts of GROMACS. Root mean square deviation (RMSD), root-mean-square fluctuation (RMSF), radius of gyration (Rg) and solvent accessible surface area (SASA) of all the three simulated proteins were analysed to check stability of the systems. RMSD was evaluated using *gmx rmsd* to study the convergence of the simulations. To calculate the RMSF for deviation in the position of atoms, *gmx rmsf* was used. Rg was calculated to measure the protein folding and compactness by using *gmx gyrate*. The SASA gives an idea of the area of the amino acids exposed to the surface, as measured by using *gmx sasa*. The number of hydrogen bonds present within the three nsp1 was analyzed through *gmx hbond* with default parameters. The subsequent analyses were performed using GROMACS utilities, VMD [40], USCF Chimera [41], Pymol [42], and also the plots were created using xmgrace [43].

2.8 Principal components analysis (PCA) or essential dynamics

Principal components analysis or essential dynamics is a process which extracts the essential motions from the MD trajectory of the targeted protein molecule [44]. The nsp1 protein of SARS-COV1, SARS-COV2 and MERS-COV are used for this purpose. The initial step of PCA analysis is to construct the covariance matrix which examines the linear relationship of atomic fluctuations for individual atomic pairs. The diagonalization of covariance matrix results in a matrix of eigenvectors and eigenvalues. The eigenvectors determine the movement of atoms having corresponding eigenvalues which represents the energetic contribution of an atom participating in motion. The covariance matrix and eigenvectors were analyzed using the *gmx cover* and *gmx anaeig* tool respectively. Gibbs free-energy landscape (FEL) elaborates the protein dynamic processes by representing the conformational states and the energy barriers [45]. The FEL of SARS-COV1, SARS-COV2 and MERS-COV was constructed based on the first (PC1) and second (PC2) principal components. FEL was calculated and plotted by using *gmx sham* and *gmx xpm2ps* module of GROMACS.

2.9 Protein-protein docking

The molecular interactions of nsp1 protein of SERS-COV2 (COVID-19) with the catalytic subunit of human DNA polymerase alpha, POLA1 was analyzed by using the HADDOCK (High Ambiguity Driven protein-protein DOCKing) programme. It is a flexible docking approach for the modelling of biomolecular complexes. It encodes instruction from predicted or identified protein interfaces in ambiguous interaction restraints (AIRs) to drive the docking procedure [46]. The coordinates of the solved structure of the catalytic domain of DNA polymerase alpha, POLA1 was downloaded from PDB database (PDB ID: 6AS7) and prepared for the docking experiments by removing water, ions and the ligands. The interface residues were utilized for the docking procedure. The active residues of POLA1 (Asp860, Ser863, Leu864, Arg922, Lys926, Lys950, Asn954 and Asp1004) were retrieved from the literature [47]. The active residues (Leu16, Leu18, Phe31, Val35, Glu36, Leu39, Arg43, Leu46, Gly49, Iso71, Pro109, Arg119, Val121 and Leu123) of nsp1 of SARS-COV2 were predicted from COACH server. The amino acids surrounding the active residues of both proteins were selected as passive in docking procedure. Active residues are the amino acids from the interface region of the two proteins that take

part in direct binding with the other protein partner while passive residues are the amino acids that can interact indirectly in docking procedure. Approximately 163 structures in 8 clusters were obtained from HADDOCK server, which represented 81.5% of the water-refined models. PRODIGY software [48] was used to predict the binding affinity and dissociation constant for each nsp1-POLA1 complex from the best three clusters. PISA server (http://www.ebi.ac.uk/msd-srv/prot_int/) was used to calculate total buried surface area, nature of interactions and amino acids involved in interactions at interface region.

3. Results and discussion

3.1 Sequence analysis and protein structure prediction

The sequence identity of nsp1 protein of SARS-COV2 with SARS-COV1 and MERS-COV was 84.4% and 20.61% respectively. Multiple sequence alignment (MSA) of nsp1 proteins was performed to identify the conserved residues. The amino acids marked as asterisk illustrate the positions of nsp1 protein that were highly conserved over the evolutionary time scale. The differences in the amino acid changes were also recorded. It was observed that compared to SARS-COV1 there were 28 mutations in the nsp1 protein of SARS-COV2 (**Fig. 1**). The three dimensional structure of nsp1 of SARS-COV2 and MERS-COV was modelled using the I-TASSER web server (**Fig. 2**) The highly significant templates used in the modelling of the nsp1 protein of SARS-COV2 and MERS-COV through I-TASSER are listed in **Table 1**. It was evident from the high Z score (>1 means good alignment) and good coverage in case of most of the structural templates, the generated threading alignment predicts a good and confident model in both cases. The stereochemical quality of the model nsp1 proteins was validated on the basis of Ramachandran analysis of ψ/φ angle from PROCHECK. Examination of Ramachandran plot of nsp1 protein of SARS-COV2 and MERS-COV showed above 92% residues lie in the allowed regions (**Table S1**). From ProSA and ProQ analysis, it is clear that the overall model quality of the nsp1 protein of SARS-COV2 and MERS-COV are within the range of scores typically found for proteins of similar size (**Table S1).** The important residues of the nsp1 protein of SARS-COV1, SARS-COV2 and MERS-COV that are involved in the ligand binding process are listed in **Table 2.**

3.2 Defining T-cell and linear B-cell epitopes

Several studies revealed that specific T-cell response is required for the elimination of several viral infections such as influenza A, SARS-COV, MERS-COV and para-influenza. These studies conclude that T-cell mediated response is essential for the development of specific vaccine [49,50]. $CD8^+$ cytotoxic T-cells recognize the infected cells in the lungs whereas $CD4^+$ helper T-cells are essential for the production of specific antibodies against viruses. Here we used Rank-Pep server to predict peptide binders to MHC class I and MHC class II alleles from nsp1 protein sequences by using Position Specific Scoring Matrices (PSSMs). The antigenic epitopes of three nsp1 proteins with high binding affinity were predicted and summarized in **Table 3 and Table 4**. Secreted neutralising antibodies play an important role to protect the body against viruses. The entry process of the viruses is blocked by the SARS-COV specific neutralizing antibodies [51]. The Bepipred web server was employed for the linear B-cell epitope prediction study. SARS-COV1, SARS-COV2 and MERS-COV nsp1 proteins were used for this purpose. The Kolaskar & Tongaonkar Antigenicity method was employed for the cross-checking of the predicted epitopes. The linear B-cell epitopes of the three nsp1 proteins are depicted in **Table 5**. Both humoral and cellular immune responses are important factor against coronavirus infection [50]. Finally, in SARS-COV2 nsp1 protein, four epitope rich regions (15-27, 45-81, 121-140 and 147-178) that were shared between T-cell and B-cell were reported. This information will be helpful in vaccine designing study by targeting SARS-COV2 nsp1 protein.

3.3 MD simulation analysis

Conformational stability and structural changes of three nsp1 proteins were measured by several parameters. The average value of backbone RMSD of SARS-COV1, SARS-COV2 and MERS-COV was 0.18 nm, 0.25 nm and 0.37 nm, respectively, which remained stable throughout the simulation run (**Fig. 3A**). SASA analysis suggested that the exposure of the three nsp1 protein surfaces to the solvent and the changes in solvent accessibility could lead to conformational changes of the nsp1 proteins. **Fig. 3B** shows the variations in SASA for the SARS-COV1, SARS-COV2 and MERS-COV nsp1 protein with respect to simulation time. The average value of SASA of SARS-COV1, SARS-COV2 and MERS-COV was 68 nm^2, 108 nm^2, and 110 nm^2 ,

respectively. The SASA values for the SARS-COV1 were reduced when compared with the case of SARS-COV2 and MERS-COV. The increased SASA values of SARS-COV2 and MERS-COV nsp1 protein suggest a partial unfolding of the protein structure upon exposure to solvent. Radius of gyration (Rg) is detected as root mean square deviation between the center of gravity of the respected protein and its end. It detects the stability and firmness of the simulation system and changes over simulation time due to protein folded-unfolded states.[52] The average Rg value was 1.35 nm, 1.75 nm and 1.6 nm for SARS-COV1, SARS-COV2 and MERS-COV respectively. The gyration curve showed a decrease in the overall Rg value of the SARS-COV1 nsp1 protein compared with the SARS-COV2 and MERS-COV, indicating that nsp1 protein of SARS-COV1 was in a compactly packed state and had stable folding (**Fig. 3C**). The gyration analysis of SARS-COV1, SARS-COV2 and MERS-COV nsp1 protein indicates that no significant drift was observed throughout the simulation run. The high RMSF values of SARS-COV2 indicated a larger degree of flexibility in this protein compared with SARS-COV1 and MERS-COV (**Fig. 3D**). An overall trend of backbone RMSD, SASA, radius of gyration and RMSF indicated that all three nsp1 protein systems were well equilibrated and stable during the simulation run. The formation of hydrogen bonds as a function of simulation time was also analyzed. The average number of hydrogen bonds of SARS-COV1, SARS-COV2 and MERS-COV were 65±8, 90± 5 and 110± 10, respectively **(Fig. 4)**.

3.4 Principal component analysis (PCA) and Gibbs free energy landscape (FEL)

The overall pattern of motion of the atoms was monitored using the MD trajectories projected on first (PC1) and second (PC2) principal components to gain a better understanding of the conformational changes in SARS-COV1, SARS-COV2 and MERS-COV. The eigen vectors described the collective motion of the atoms, while the eigenvalues signified the atomic influence in movement. A large distribution of lines indicated greater variance in accordance with more conformational changes in the SARS-COV2 nsp1 protein compared with SARS-COV1 and MERS-COV nsp1 protein. The trajectories of SARS-COV2 nsp1 protein covered a wider conformational space and showed higher space magnitudes. It was suggested that SARS-COV2 nsp1 protein appeared to cover a larger conformational space due to its greater flexibility when compared with

the other two nsp1 proteins (**Fig. 5**). Gibbs free energy landscape (FEL) was calculated using PC1 and PC2 coordinates of the three nsp1 protein molecules. The ΔG values for SARS-COV1, SARS-COV2 and MERS-COV nsp1 protein were 4.44, 5.82 and 6.15 kJ/mol respectively. The blue, cyan and green regions in the free energy landscape plot denote low energy states with highly stable protein conformation while the red region signify high energy states with unstable protein conformation. Conformational stability of the three nsp1 proteins with lower free energy (global minima) can be inferred by a smaller and more concentrated blue colour (**Fig. 6**).

3.5. Molecular interactions of SARS-COV2 nsp1 with POLA1

The catalytic domain of DNA polymerase alpha, POLA1 is involved in the replication process. The molecular association of SARS-COV2 nsp1 with POLA1 was predicted by the HADDOCK programme. The nsp1-POLA1 docked complexes were analyzed based on Z-score and HADDOCK score (**Fig. 7 & Table S2**). PRODIGY was used to predict the binding energy for each nsp1-POLA1 complex from the best there cluster. Three best docked complexes were selected on the basis of lowest binding energy. (**Fig. S1**). The best energy values obtained were -13.0 kcal/mol, -11.6 kcal/mol and -9.6 kcal/mol. **(Table S2).** Interface area, involvement of amino acids and molecular interactions were calculated by PISA server. The interface area of the best docked complex (ΔG = -13.0 kcal/mol) was 1260.9 $Å^2$ and shown in **Fig. 8A.** Interaction studies of this nsp1-POLA1 complex showed thirteen hydrogen bonds and eight salt bridge interactions at the interface region (**Table 6** & **Fig. 8B**). It was observed from the docking experiments that the residues of finger domain (Lys923, Gln927, Gln932) and palm domain (Glu1060, Lys1020, Lys1024, Asn1030, Lys1031 and Glu1037) of POLA1 are mainly involved in the binding process with SARS-COV2 nsp1 protein (**Fig. 7**). The hydrogen bonds and salt bridges interactions play an important role towards the stability of the SARS-COV2 nsp1-POLA1 complex formation.

4. Conclusion

COVID-19 pandemic leads to a health, economic, social and political crisis in the world. The development of a specific targeted therapy could reduce the rate of infection. This comprehensive study represents an immunoinformatics approach towards the identification of specific B-

cell and T-cell epitopes of three nsp1 protein. Four epitope rich regions (15-27, 45-81, 121-140 and 147-178) that were shared between T-cell and B-cell were reported in SARS-COV2 nsp1 protein. The in-depth structural elucidation of nsp1 proteins together with dynamic conformations showed that SARS-COV2 nsp1 protein covers a large conformational space due to its greater flexibility compared with SARS-COV1 and MERS-COV. A three-dimensional structural model of the complex structure between SARS-COV2 nsp1 protein and catalytic subunit of DNA polymerase alpha POLA1 was constructed using protein-protein docking approach. During complex formation between SARS-COV2 nsp1 and POLA1, salt bridge interactions help to bring the two proteins in close proximity and form 13 strong hydrogen bonds that contribute to the stability of the complex formation. Knowledge of this important binding site could open the door for further simulation and experimental studies on the mode of SARS-COV2 nsp1 protein recognition by the catalytic site of DNA polymerase alpha POLA1. Taken all together, according to structural evaluation as well as immunological analysis, nsp1 protein could be considered as a possible drug target and candidate molecule for the vaccine development process against COVID-19.

Acknowledgement

The author wishes to express sincere thanks to Dr. Sibani Sen Chakraborty for her useful suggestions in preparation of the manuscript.

Conflict of Interest statement

The authors declare that they have no known competing financial interests or personal relationships that could have appeared to influence the work reported in this paper.

Data Availability

The modelled and docking structures are available upon request from the corresponding author.

CRediT authorship contribution statement

Ankur Chaudhuri: Supervision, Conceptualization, Formal analysis, Writing - review & editing.

Funding

This research did not receive any specific grant from funding agencies in the public, commercial, or not-for-profit sectors.

References:

1. Lu Roujian, Zhao Xiang, Li Juan, Niu Peihua, Yang Bo, Wu Honglong, et al. Genomic characterisation and epidemiology of 2019 novel coronavirus: implications for virus origins and receptor binding. *The Lancet* 2020;**395**(10224):565–74. Doi: 10.1016/s0140-6736(20)30251-8
2. Wu Fan, Zhao Su, Yu Bin, Chen Yan-Mei, Wang Wen, Song Zhi-Gang, et al. A new coronavirus associated with human respiratory disease in China. *Nature* 2020;**579**(7798):265–9. Doi: 10.1038/s41586-020-2008-3.
3. (worldometers.info. (2020). COVID-19 coronavirus pandemic. https://www. worldometers.info/coronavirus/ (Last accessed May 25, 2020)
4. Elfiky Abdo A., Mahdy Samah M., Elshemey Wael M. Quantitative structure-activity relationship and molecular docking revealed a potency of anti-hepatitis C virus drugs against human corona viruses. *Journal of Medical Virology* 2017;**89**(6):1040–7. Doi: 10.1002/jmv.24736.
5. Bogoch Isaac I, Watts Alexander, Thomas-Bachli Andrea, Huber Carmen, Kraemer Moritz U G, Khan Kamran. Potential for global spread of a novel coronavirus from China. *Journal of Travel Medicine* 2020;**27**(2). Doi: 10.1093/jtm/taaa011.
6. Woo Patrick C. Y., Huang Yi, Lau Susanna K. P., Yuen Kwok-Yung. Coronavirus Genomics and Bioinformatics Analysis. *Viruses* 2010;**2**(8):1804–20. Doi: 10.3390/v2081803.
7. Ahmed Syed Faraz, Quadeer Ahmed A., Mckay Matthew R. Preliminary Identification of Potential Vaccine Targets for the COVID-19 Coronavirus (SARS-CoV-2) Based on SARS-CoV Immunological Studies. *Viruses* 2020;**12**(3):254. Doi: 10.3390/v12030254.

8. Gordon, D.E., Jang, G.M., Bouhaddou, M. et al. A SARS-CoV-2 protein interaction map reveals targets for drug repurposing. *Nature* 2020. Doi: 10.1038/s41586-020-2286-9
9. Neuman Benjamin W., Chamberlain Peter, Bowden Fern, Joseph Jeremiah. Atlas of coronavirus replicase structure. *Virus Research* 2014;**194**:49–66. Doi: 10.1016/j.virusres.2013.12.004.
10. Connor Ramsey F., Roper Rachel L. Unique SARS-CoV protein nsp1: bioinformatics, biochemistry and potential effects on virulence. *Trends in Microbiology* 2007;**15**(2):51–3. Doi: 10.1016/j.tim.2006.12.005.
11. Kamitani Wataru, Huang Cheng, Narayanan Krishna, Lokugamage Kumari G, Makino Shinji. A two-pronged strategy to suppress host protein synthesis by SARS coronavirus Nsp1 protein. *Nature Structural & Molecular Biology* 2009;**16**(11):1134–40. Doi: 10.1038/nsmb.1680.
12. Lokugamage K. G., Narayanan K., Huang C., Makino S. Severe Acute Respiratory Syndrome Coronavirus Protein nsp1 Is a Novel Eukaryotic Translation Inhibitor That Represses Multiple Steps of Translation Initiation. *Journal of Virology* 2012;**86**(24):13598–608. Doi: 10.1128/jvi.01958-12.
13. Channappanavar Rudragouda, Fehr Anthony R., Vijay Rahul, Mack Matthias, Zhao Jincun, Meyerholz David K., et al. Dysregulated Type I Interferon and Inflammatory Monocyte-Macrophage Responses Cause Lethal Pneumonia in SARS-CoV-Infected Mice. *Cell Host & Microbe* 2016;**19**(2):181–93. Doi: 10.1016/j.chom.2016.01.007.
14. Kindler Eveline, Thiel Volker. SARS-CoV and IFN: Too Little, Too Late. *Cell Host & Microbe* 2016;**19**(2):139–41. Doi: 10.1016/j.chom.2016.01.012.
15. Law Anna H. Y., Lee Davy C. W., Cheung Benny K. W., Yim Howard C. H., Lau Allan S. Y. Role for Nonstructural Protein 1 of Severe Acute Respiratory Syndrome Coronavirus in Chemokine Dysregulation. *Journal of Virology* 2006;**81**(1):416–22. Doi: 10.1128/jvi.02336-05.
16. NCBI. National Center of Biotechnology Informatics (NCBI) database website http://www.ncbi.nlm.nih.gov/. 2020. http://www.ncbi.nlm.nih.gov/2020

17. Gish Warren, States David J. Identification of protein coding regions by database similarity search. *Nature Genetics* 1993;**3**(3):266–72. Doi: 10.1038/ng0393-266.
18. Notredame Cédric, Higgins Desmond G, Heringa Jaap. T-coffee: a novel method for fast and accurate multiple sequence alignment 1 1Edited by J. Thornton. *Journal of Molecular Biology* 2000;**302**(1):205–17. Doi: 10.1006/jmbi.2000.4042.
19. Almeida Marcius S., Johnson Margaret A., Herrmann Torsten, Geralt Michael, Wüthrich Kurt. Novel β-Barrel Fold in the Nuclear Magnetic Resonance Structure of the Replicase Nonstructural Protein 1 from the Severe Acute Respiratory Syndrome Coronavirus. *Journal of Virology* 2007;**81**(7):3151–61. Doi: 10.1128/jvi.01939-06.
20. Yang Jianyi, Yan Renxiang, Roy Ambrish, Xu Dong, Poisson Jonathan, Zhang Yang. The I-TASSER Suite: protein structure and function prediction. *Nature Methods* 2014;**12**(1): 7–8. Doi: 10.1038/nmeth.3213.
21. Zheng Wei, Zhang Chengxin, Wuyun Qiqige, Pearce Robin, Li Yang, Zhang Yang. LOMETS2: improved meta-threading server for fold-recognition and structure-based function annotation for distant-homology proteins. *Nucleic Acids Research* 2019;**47**(W1). Doi: 10.1093/nar/gkz384.
22. Cozzetto Domenico, Kryshtafovych Andriy, Tramontano Anna. Evaluation of CASP8 model quality predictions. *Proteins: Structure, Function, and Bioinformatics* 2009;**77**(S9):157–66. Doi: 10.1002/prot.22534.
23. Laskowski R. A., Macarthur M. W., Moss D. S., Thornton J. M. PROCHECK: a program to check the stereochemical quality of protein structures. *Journal of Applied Crystallography* 1993;**26**(2):283–91. Doi: 10.1107/s0021889892009944.
24. Morris Anne Louise, Macarthur Malcolm W., Hutchinson E. Gail, Thornton Janet M. Stereochemical quality of protein structure coordinates. *Proteins: Structure, Function, and Genetics* 1992;**12**(4):345–64. Doi: 10.1002/prot.340120407.
25. Wiederstein M., Sippl M. J. ProSA-web: interactive web service for the recognition of errors in three-dimensional structures of proteins. *Nucleic Acids Research* 2007;**35**(Web Server). Doi: 10.1093/nar/gkm290.

26. Cristobal Susana, Zemla Adam, Fischer Daniel, Rychlewski Leszek, Elofsson Arne. A study of quality measures for protein threading models. *BMC Bioinformatics* 2001;**2**(1):5. Doi: 10.1186/1471-2105-2-5.

27. Yang Jianyi, Roy Ambrish, Zhang Yang. Protein–ligand binding site recognition using complementary binding-specific substructure comparison and sequence profile alignment. *Bioinformatics* 2013;**29**(20):2588–95. Doi: 10.1093/bioinformatics/btt447.

28. Yang Jianyi, Roy Ambrish, Zhang Yang. BioLiP: a semi-manually curated database for biologically relevant ligand–protein interactions. *Nucleic Acids Research* 2012;**41**(D1). Doi: 10.1093/nar/gks966.

29. Reche Pedro A., Reinherz Ellis L. Prediction of Peptide-MHC Binding Using Profiles. *Methods in Molecular Biology Immunoinformatics* 2007:185–200. Doi: 10.1007/978-1-60327-118-9_13.

30. Kruiswijk Corine, Richard Guilhem, Salverda Merijn L.m., Hindocha Pooja, Martin William D., Groot Anne S. De, et al. In silico identification and modification of T cell epitopes in pertussis antigens associated with tolerance. *Human Vaccines & Immunotherapeutics* 2020;**16**(2):277–85. Doi: 10.1080/21645515.2019.1703453.

31. Vita Randi, Mahajan Swapnil, Overton James A, Dhanda Sandeep Kumar, Martini Sheridan, Cantrell Jason R, et al. The Immune Epitope Database (IEDB): 2018 update. *Nucleic Acids Research* 2018;**47**(D1). Doi: 10.1093/nar/gky1006.

32. Kolaskar A.s., Tongaonkar Prasad C. A semi-empirical method for prediction of antigenic determinants on protein antigens. *FEBS Letters* 1990;**276**(1-2):172–4. Doi: 10.1016/0014-5793(90)80535-q.

33. Mirza Muhammad Usman, Rafique Shazia, Ali Amjad, Munir Mobeen, Ikram Nazia, Manan Abdul, et al. Towards peptide vaccines against Zika virus: Immunoinformatics combined with molecular dynamics simulations to predict antigenic epitopes of Zika viral proteins. *Scientific Reports* 2016;**6**(1). Doi: 10.1038/srep37313.

34. Berendsen H.j.c., Spoel D. Van Der, Drunen R. Van. GROMACS: A message-passing parallel molecular dynamics implementation. *Computer Physics Communications* 1995;**91**(1-3):43–56. Doi: 10.1016/0010-4655(95)00042-e.

35. Jorgensen William L., Maxwell David S., Tirado-Rives Julian. Development and Testing of the OPLS All-Atom Force Field on Conformational Energetics and Properties of Organic Liquids. *Journal of the American Chemical Society* 1996;**118**(45):11225–36. Doi: 10.1021/ja9621760.
36. Jorgensen William L., Chandrasekhar Jayaraman, Madura Jeffry D., Impey Roger W., Klein Michael L. Comparison of simple potential functions for simulating liquid water. *The Journal of Chemical Physics* 1983;**79**(2):926–35. Doi: 10.1063/1.445869.
37. Parrinello M., Rahman A. Polymorphic transitions in single crystals: A new molecular dynamics method. *Journal of Applied Physics* 1981;**52**(12):7182–90. Doi: 10.1063/1.328693.
38. Essmann Ulrich, Perera Lalith, Berkowitz Max L., Darden Tom, Lee Hsing, Pedersen Lee G. A smooth particle mesh Ewald method. *The Journal of Chemical Physics* 1995;**103**(19):8577–93. Doi: 10.1063/1.470117.
39. Hess Berk, Bekker Henk, Berendsen Herman J. C., Fraaije Johannes G. E. M. LINCS: A linear constraint solver for molecular simulations. *Journal of Computational Chemistry* 1997;**18**(12):1463–72. Doi: 10.1002/(sici)1096-987x(199709)18:12<1463::aid-jcc4>3.0.co;2-h.
40. Humphrey William, Dalke Andrew, Schulten Klaus. VMD: Visual molecular dynamics. *Journal of Molecular Graphics* 1996;**14**(1):33–8. Doi: 10.1016/0263-7855(96)00018-5.
41. Pettersen Eric F., Goddard Thomas D., Huang Conrad C., Couch Gregory S., Greenblatt Daniel M., Meng Elaine C., et al. UCSF Chimera?A visualization system for exploratory research and analysis. *Journal of Computational Chemistry* 2004;**25**(13):1605–12. Doi: 10.1002/jcc.20084.
42. DeLano WL. PyMOL: an open-source molecular graphics tool. *Ccp4 Newslett Protein Crystallogr* 2002;40:11
43. Turner PJ. XMGRACE, Version 5.1.19. 2005; Central for costal and Land-Margin Research; Oregon Graduate Institute of Science and Technology, Beaverton, ORE, USA

44. Amadei Andrea, Linssen Antonius B. M., Berendsen Herman J. C. Essential dynamics of proteins. *Proteins: Structure, Function, and Genetics* 1993;**17**(4):412–25. Doi: 10.1002/prot.340170408.

45. Frauenfelder H, Sligar S., Wolynes P. The energy landscapes and motions of proteins. *Science* 1991;**254**(5038):1598–603. Doi: 10.1126/science.1749933.

46. Zundert G.c.p. Van, Rodrigues J.p.g.l.m., Trellet M., Schmitz C., Kastritis P.l., Karaca E., et al. The HADDOCK2.2 Web Server: User-Friendly Integrative Modeling of Biomolecular Complexes. *Journal of Molecular Biology* 2016;**428**(4):720–5. Doi: 10.1016/j.jmb.2015.09.014.

47. Tahirov T.h., Baranovskiy A.g., Babayeva N.d. Crystal Structure Of The Catalytic Core Of Human Dna Polymerase Alpha In Ternary Complex With An Dna-Primed Dna Template And Dctp 2018. Doi: 10.2210/pdb6as7/pdb.

48. Xue Li C., Rodrigues João Pglm, Kastritis Panagiotis L., Bonvin Alexandre Mjj, Vangone Anna. PRODIGY: a web server for predicting the binding affinity of protein–protein complexes. *Bioinformatics* 2016. Doi: 10.1093/bioinformatics/btw514.

49. Channappanavar Rudragouda, Zhao Jincun, Perlman Stanley. T cell-mediated immune response to respiratory coronaviruses. *Immunologic Research* 2014;**59**(1-3):118–28. Doi: 10.1007/s12026-014-8534-z.

50. Oh Hsueh-Ling Janice, Gan Samuel Ken-En, Bertoletti Antonio, Tan Yee-Joo. Understanding the T cell immune response in SARS coronavirus infection. *Emerging Microbes & Infections* 2012;**1**(1):1–6. Doi: 10.1038/emi.2012.26.

51. Hsueh P.-R., Huang L.-M., Chen P.-J., Kao C.-L., Yang P.-C. Chronological evolution of IgM, IgA, IgG and neutralisation antibodies after infection with SARS-associated coronavirus. *Clinical Microbiology and Infection* 2004;**10**(12):1062–6. Doi: 10.1111/j.1469-0691.2004.01009.x.

52. Ivankov Dmitry N., Bogatyreva Natalya S., Lobanov Michail Yu, Galzitskaya Oxana V. Coupling between Properties of the Protein Shape and the Rate of Protein Folding. *PLoS ONE* 2009;**4**(8). Doi: 10.1371/journal.pone.0006476.

Figure legends:

Fig 1: Multiple sequence alignment for nsp1 protein of SARS-COV1, SARS-COV2 and MERS-COV. The alignment is shown using the Clustal Omega web server. Asterisk represents the conserved residues. Mutated residues of SARS-COV2 nsp1 protein are represented as red box

Fig 2: Prediction of three dimensional structure of nsp1 protein by I-TASSER programme. A. Modelled structure of SARS-COV2 nsp1 protein. B. Modelled structure of MERS-COV nsp1 protein. C. Superimposition of SARS-COV1 (PDB ID: 2hsx) with SARS-COV2 and MERS-COV nsp1

Fig 3: Analysis of MD simulation of three nsp1 proteins. A. Root mean square deviation (RMSD). B. Solvent accessible surface area (SASA). C. Radius of gyration. D. Root mean square fluctuations (RMSF). Black, red and green colour represents the SARS-COV1, SARS-COV2 and MERS-COV nsp1 , respectively

Fig. 4: Trajectory analysis of hydrogen bonds. Hydrogen bonds are responsible for the stability of the protein molecules. Black, red and green colour depicts the number of hydrogen bonds of the the SARS-COV1, SARS-COV2 and MERS-COV, respectively thought the simulation run

Fig. 5: Projection of motion of nsp1 protein atoms of SARS-COV1 (Black colour), SARS-COV2 (red colour) and MERS-COV (green colour) on PC1 and PC2

Fig. 6: Gibbs free energy landscape (FEL) plot of three nsp1 proteins. A. SARS-COV1. B. SARS-COV2. C. MERS-COV. The blue, cyan and green regions in the free energy landscape plot denotes low energy state with highly stable protein conformation while the red region signify high energy state with unstable protein conformation

Fig. 7: The structure of docking complex between SARS-COV2 nsp1 protein and POLA1. SARS-COV2 nsp1 is represented by a yellow cartoon. POLA1 is composed of five domains. N-terminal (338-534 & 761-808), exonuclease (535-760), palm (834-908 & 968-1076), finger (909-967), and thumb (1077-1250) domain are represented by pale green, orange, cyan, magenta and

grey colour respectively. The binding affinity of nsp1 is higher at the interface region of palm (cyan colour) and finger (magenta colour) domain of POLA1

Fig. 8: The proposed binding mode of the host cell POLA1 and the COVID-19 nsp1 model. A. Nsp1 (yellow surface) interacts with the palm (cyan surface) and finger (magenta surface) domain. Interface region is represented by a red surface. B. Molecular interactions between SARS-COV2 nsp1 and POLA1. Interface residues are represented as a line model. Several bonds are depicted by orange dotted line

Table legends:

Table 1: The highly significant structural templates for sequence alignment obtained from PDB library for modelling through I-TASSER

Table 2: Active residues prediction by COACH server

Table 3: HLA I antigenic epitopes predicted using Rankpep

Table 4: HLA II antigenic epitopes predicted using Rankpep

Table 5: Predicted linear B-cell epitopes of SARS-COV1, SARS-COV2 and MERS-COV nsp1 proteins via Bepipred and Kolaskar & Tongaonkar antigenicity

Table 6: Intermolecular interactions of the best docked complex of nsp1-POLA1 predicted by PISA analysis

Supplementary

Fig. S1: Best SARS-COV2 nsp1-POLA1 complex model. A. Top model from Cluster1. B. Top model from cluster2. C. Top model from cluster5. Best model from each cluster was predicted according to lowest binding energy. Binding affinity is calculated by PRODIGY server

Table S1: Three-dimensional model validation using several analyses

Table S2: Protein-protein docking between SARS-COV2 nsp1 and POLA1 by HADDOCK server

Highlights:

- Structural elucidation at molecular level of nsp1 of SARS-COV1, SARS-COV2, and MERS-COV
- Identifications of epitopes by immunoinformatics approach
- SARS-COV2 nsp1 cover a large conformational space due to greater flexibility
- Molecular docking between SARS-COV2 nsp1 and POLA1 to identify important residues
- Structural insights of nsp1 could be used in drug design process against COVID-19

Graphical abstract

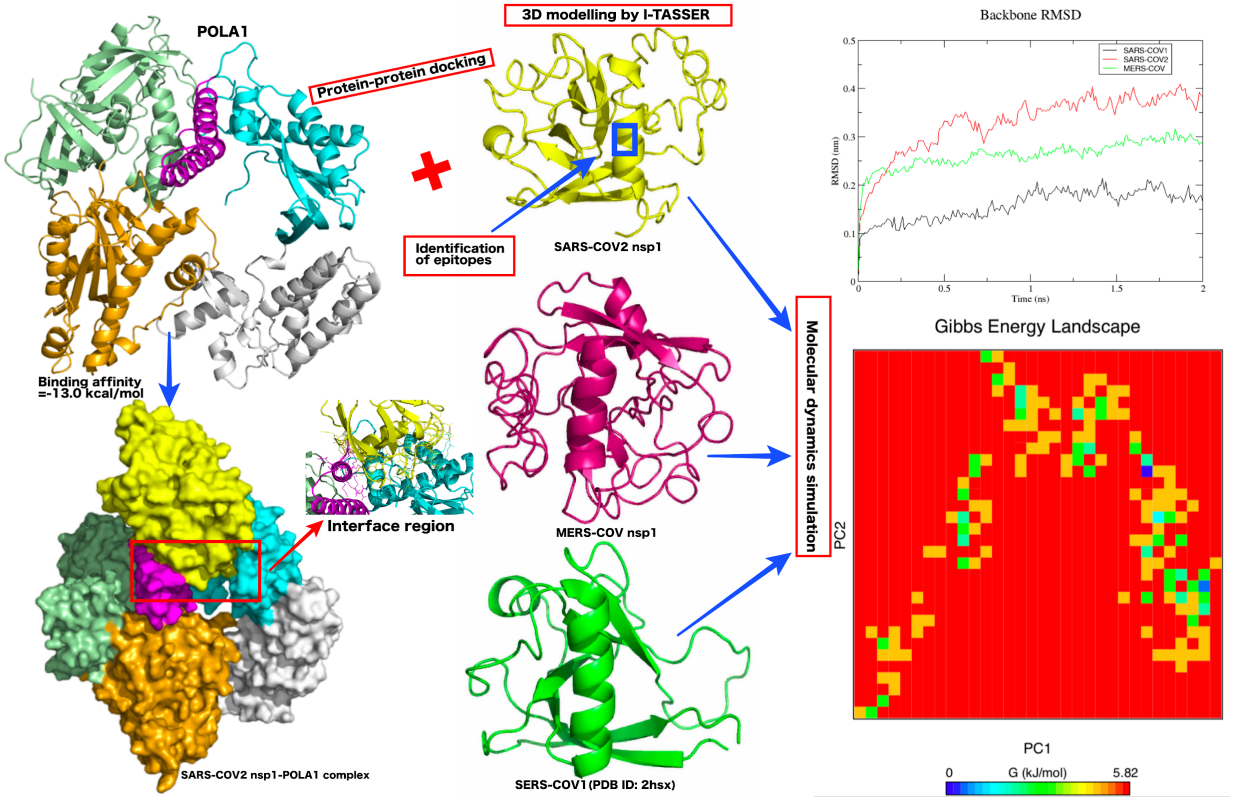

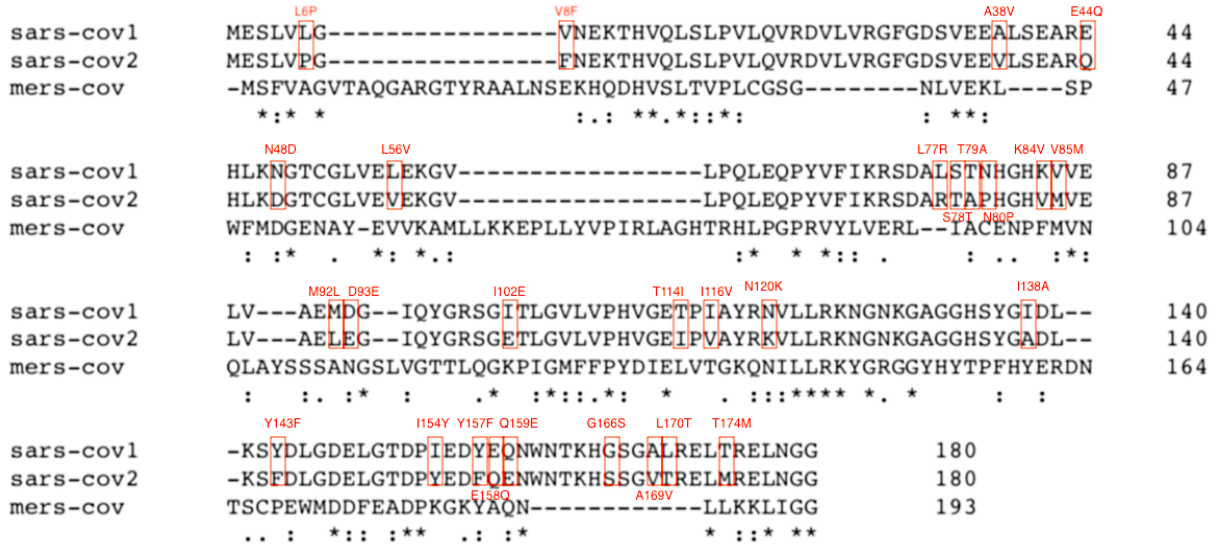

Fig 1: Multiple sequence alignment for nsp1 protein of SARS-COV1, SARS-COV2 and MERS-COV. The alignment is shown using the Clustal Omega web server. Asterisk represents the conserved residues. Mutated residues of SARS-COV2 nsp1 protein are represented as red box

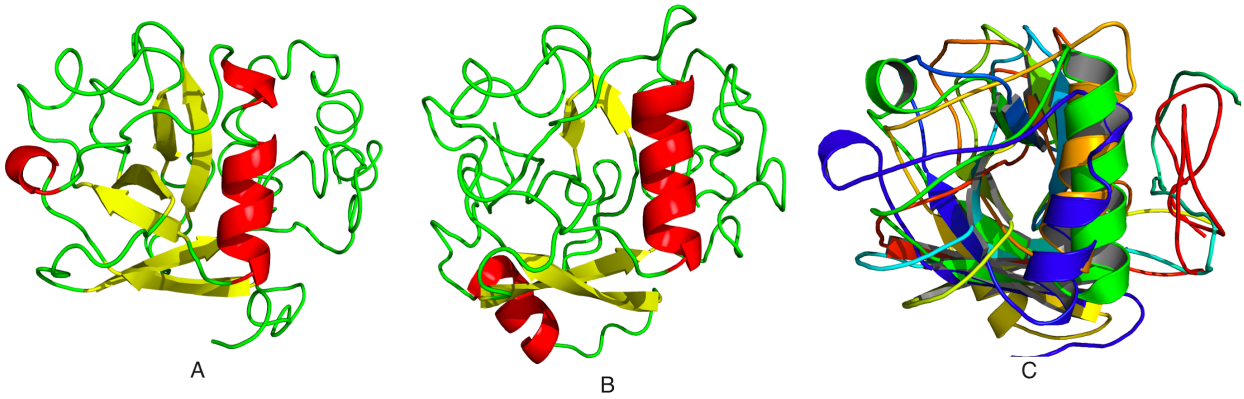

Fig 2: Prediction of three dimensional structure of nsp1 protein by I-TASSER programme. A. Modelled structure of SARS-COV2 nsp1 protein. B. Modelled structure of MERS-COV nsp1 protein. C. Superimposition of SARS-COV1 (PDB ID: 2hsx) with SARS-COV2 and MERS-COV nsp1

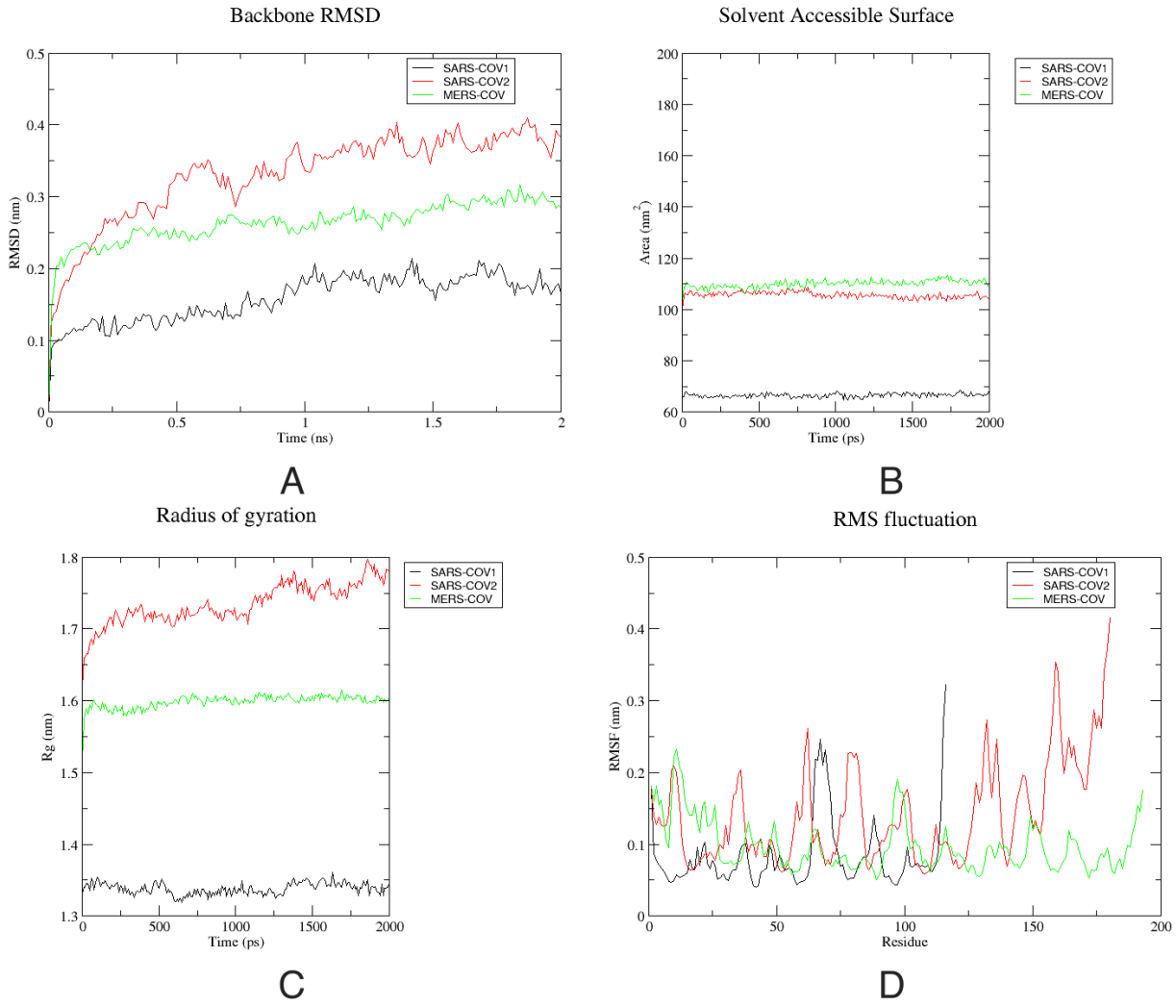

Fig 3: Analysis of MD simulation of three nsp1 proteins. A. Root mean square deviation (RMSD). B. Solvent accessible surface area (SASA). C. Radius of gyration. D. Root mean square fluctuations (RMSF). Black, red and green colour represents the SARS-COV1, SARS-COV2 and MERS-COV nsp1 , respectively

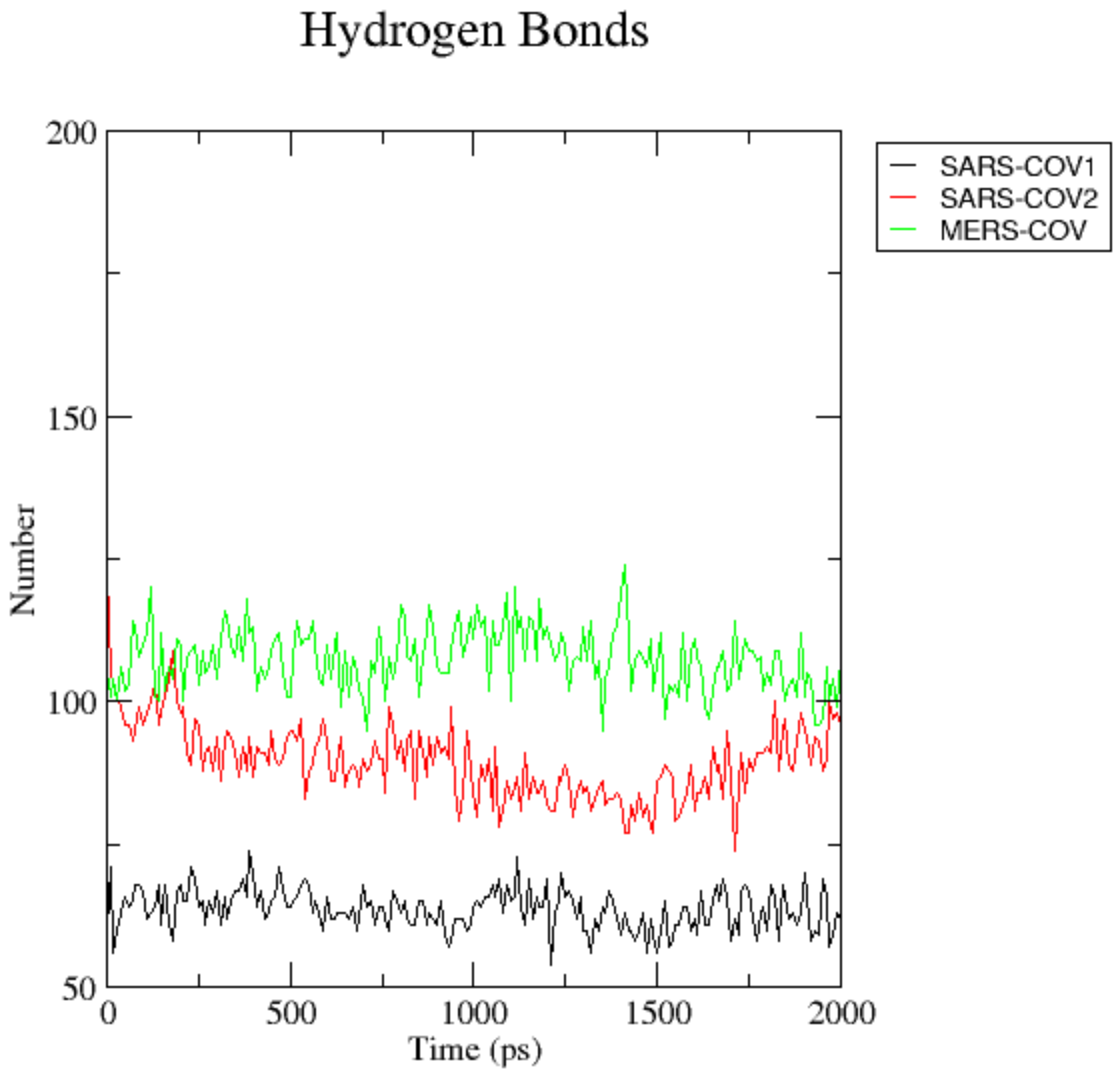

Fig. 4: Trajectory analysis of hydrogen bonds. Hydrogen bonds are responsible for the stability of the protein molecules. Black, red and green colour depicts the number of hydrogen bonds of the the SARS-COV1, SARS-COV2 and MERS-COV, respectively throughout the simulation run

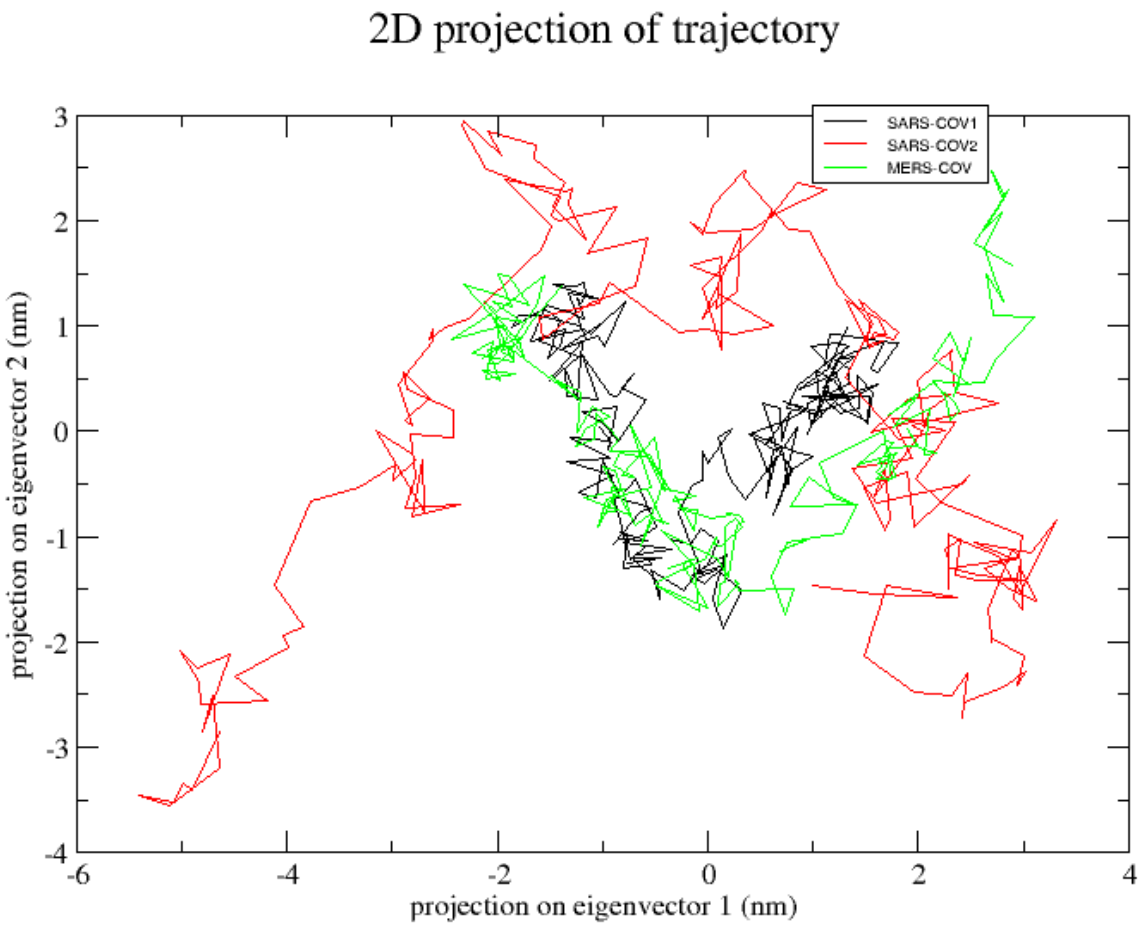

Fig. 5: Projection of motion of nsp1 protein atoms of SARS-COV1 (Black colour), SARS-COV2 (red colour) and MERS-COV (green colour) on PC1 and PC2

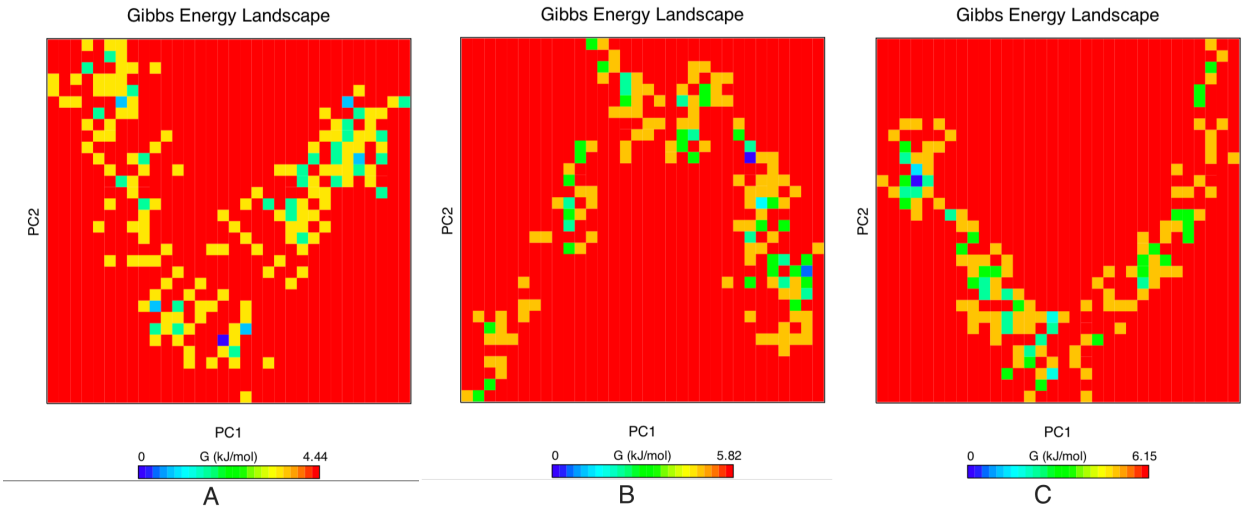

Fig. 6: Gibbs free energy landscape (FEL) plot of three nsp1 proteins. A. SARS-COV1. B. SARS-COV2. C. MERS-COV. The blue, cyan and green regions in the free energy landscape plot denotes low energy state with highly stable protein conformation while the red region signify high energy state with unstable protein conformation

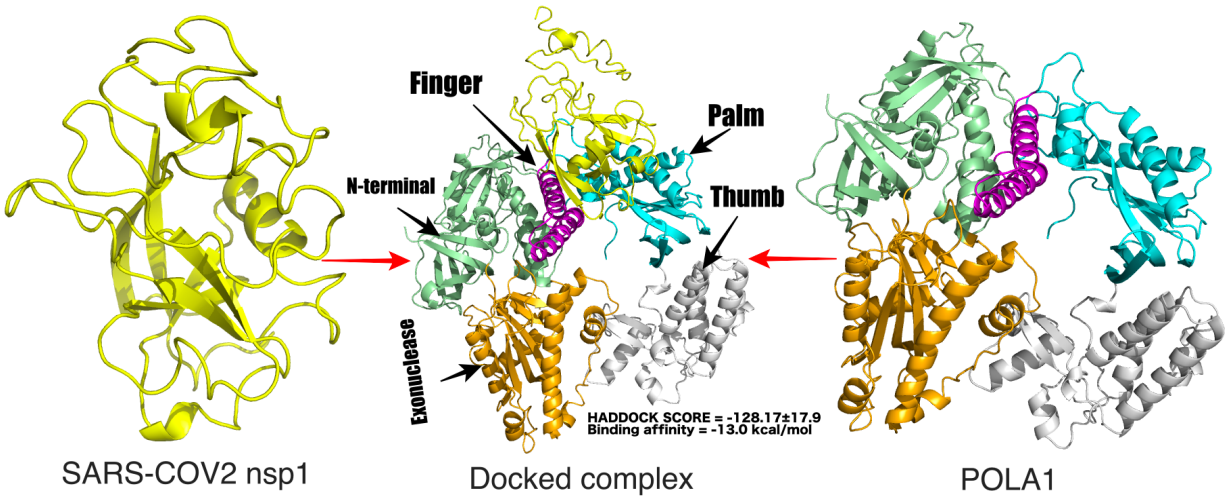

Fig. 7: The structure of docking complex between SARS-COV2 nsp1 protein and POLA1. SARS-COV2 nsp1 is represented by a yellow cartoon. POLA1 is composed of five domains. N-terminal (338-534 & 761-808), exonuclease (535-760), palm (834-908 & 968-1076), finger (909-967), and thumb (1077-1250) domain are represented by pale green, orange, cyan, magenta and grey colour respectively. The binding affinity of nsp1 is higher at the interface region of palm (cyan colour) and finger (magenta colour) domain of catalytic subunit of DNA polymerase alpha POLA1

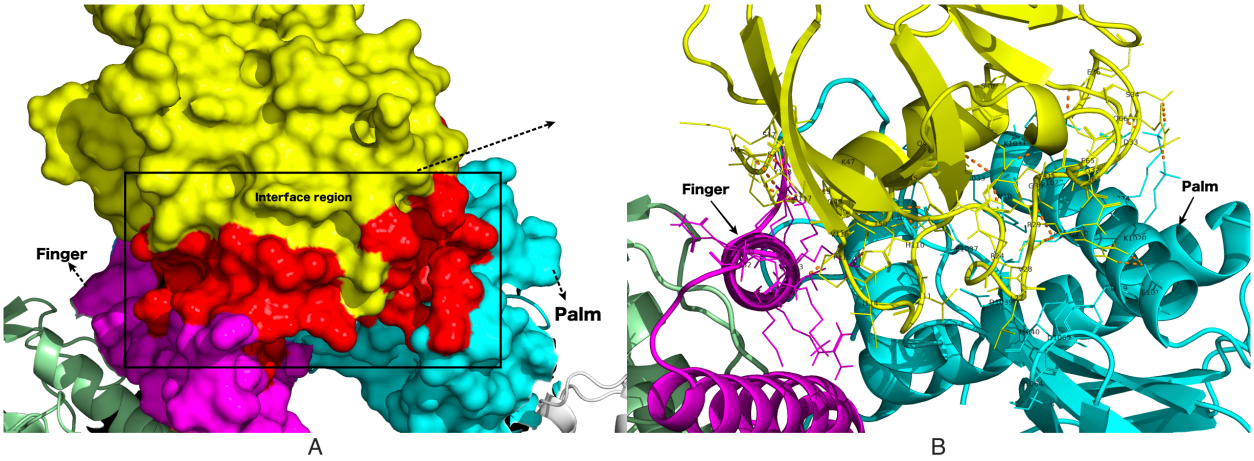

Fig. 8: The proposed binding mode of the host cell POLA1 and the COVID-19 nsp1 model. A. Nsp1 (yellow surface) interacts with the palm (cyan surface) and finger (magenta surface) domain. Interface region is represented by a red surface. B. Molecular interactions between SARS-COV2 nsp1 and POLA1. Interface residues are represented as a line model. Several bonds are depicted by orange dotted line

Table 1: The highly significant structural templates for sequence alignment obtained from PDB library for modelling through I-TASSER

SARS-COV2		**MERS-COV**	
PDB ID	Normalized Z Score	PDB ID	Normalized Z Score
2hsxA	1.83	2hsx	8.11
2gdtA	2.52	2hsx	9.76
2gdt	1.70	2hsx	5.19
2hsx	10.03	5xbc	1.43
2hsx	4.59	3zbd	1.14
2hsxA	2.14	2v0gA	0.72
2hsx	7.61	2gdtA	0.95
2gdtA	3.07	2p97A	0.63
2gdtA	2.75	1v8eA	0.60
2hsxA	2.34	3fdfA	0.69

Table 2: Active residues prediction by COACH server

Nsp1 proteins	**Active site residues**
SARS-COV1	Leu16, Leu18, Phe31, Leu39, Arg43, Leu46, Gly49, Iso71, Pro109, Arg119, Val121, Leu123
SARS-COV2	Leu16, Leu18, Phe31, Val35, Glu36, Leu39, Arg43, Leu46, Gly49, Iso71, Pro109, Arg119, Val121, Leu123
MERS-COV	Arg13

Table 3: HLA I antigenic epitopes predicted using Rankpep.

Sl.No	Alleles	SARS-COV1	SARS-COV2	MERS-COV
1	HLA_A0201	15-23 QLSLPVLQV 84-92 KVVELVAEM 103-111 TLGVLVPHV 169-177 ALRELTREL	84-92 VMVELVAEL 15-23 QLSLPVLQV 106-114 VLVPHVGEI	135-143 ELVTGKQNI 89-97 YLVERLIAC 62-70 MLLKKEPLL 75-83 RLAGHTRHL
2	HLA_A0204	78-86 STNHGHKVV	78-86 TAPHGHVMV 45-53 HLKDGTCGL	80-88 TRHLPGPRV 3-11 FVAGVTAQC
3	HLA_A0206	103-111 TLGVLVPHV 38-46 ALSEAREHL	106-114 VLVPHVGEI 103-111 TLGVLVPHV	-
4	HLA_A0301	121-129 VLLRKNGNK	121-129 VLLRKNGNK	57-66 EVVKAMLLKK
5	HLA_A11	-	-	58-66 VVKAMLLKK
6	HLA_A1101	76-84 ALSTNHGHK	3-11 SLVPGFNEK	-
7	HLA_A2402	96-104 QYGRSGITL	153-161 PYEDFQENW 96-104 QYGRSGETL	-
8	HLA_A31	116-124 IAYRNVLLR	116-124 VAYRKVLLR	154-162 HYTPFHYER
9	HLA_A6801	116-124 IAYRNVLLR 76-84 ALSTNHGHK	-	-
10	HLA_B0702	-	114-122 IPVAYRKVL	-
11	HLA_B2705	-	76-84 ARTAPHGHV	74-82 IRLAGHTRH
12	HLA_B35	-	-	124-132 KPIGMFFPV

13	HLA_B3501	61-69 LPQLEQPYV	61-69 LPQLEQPYV	33-42 VPLCGSGNLV 99-108 NPFMVNQLAY
14	HLA_B51	61-69 LPQLEQPYV 108-116 VPHVGETPI	61-69 LPQLEQPYV	83-91 LPGPRVYLV 33-41 VPLCGSGNL
15	HLA_B5101	108-116 VPHVGETPI 18-26 LPVLQVRDV	108-116 VPHVGEIPV 114-122 IPVAYRKVL 18-26 LPVLQVRDV	-
16	HLA_B5102	61-69 LPQLEQPYV 18-26 LPVLQVRDV	-	-
17	HLA_B5103	108-116 VPHVGETPI 18-26 LPVLQVRDV	18-26 LPVLQVRDV	-
18	HLA_B5401	-	-	83-91 LPGPRVYLV
19	HLA_X	169-177 ALRELTREL	-	82-90 HLPGPRVYL 124-132 KPIGMFFPY 128-136 MFFPYDIEL

Table 4: HLA II antigenic epitopes predicted using Rankpep.

Sl.No	Alleles	SARS-COV1	SARS-COV2	MERS-COV
1	HLADRB10101	68-76 YVFIKRSDA	71-79 IKRSDARTA 68-76 YVFIKRSDA	108-116 YSSSANGSL 99-107 NPFMVNQLA 3-11 FVAGVTAQG 80-88 TRHLPGPRV
2	HLADRB10401	157-165 YEQNWNTKH 97-105 YGRSGITLG 68-76 YVFIKRSDA 116-124 IAYRNVLLR	97-105 YGRSGETLG 157-165 FQENWNTKH 68-76 YVFIKRSDA 55-63 EVEKGVLPQ	3-11 FVAGVTAQG 2-10 SFVAGVTAQ 106-114 YERDNTSCP 114-122 GSLVGTTLQ
3	HLADRB10701	-	-	95-103 IACENPFMV
4	HLADRB11101	159-167 QNWNTKHGS 163-171 TKHGSGALR	159-167 ENWNTKHSS 169-177 VTRELMREL	59-67 VKAMLLKKE 182-190 YAQNLLKKL
5	HLADRB11501	54-62 VELEKGVLP 20-28 VLQVRDVLV 133-141 GHSYGIDLK	54-62 VEVEKGVLP 20-28 VLQVRDVLV 133-141 GHSYGADLK 69-77 VFIKRSDAR	126-134 IGMFFPYDI 56-64 YEVVKAMLL

Table 5: Predicted linear B-cell epitopes of SARS-COV1, SARS-COV2 and MERS-COV nsp1 protein via Bepipred and Kolaskar & Tongaonkar antigenicity.

Antigen	Server	Amino acid position	Sequence
SARS-COV1	**Bepipred**	33-60 76-79 95-97 111-116 127-135 145-168	DSVEEALS ALST IQY VGETPI GNKGAGGHS LGDELGTDPIEDYEQNWNTKHGSG
	Kolaskar & Tongaonkar	13-29 51-72 83-89 103-114 118-124 137-143	HVQLSLPVLQVRDVLVR CGLVELEKGVLPQLEQPYVFIK HKVVELV TLGVLVPHVGET YRNVLLR GIDLKSY
SARS-COV2	**Bepipred**	9-11 33-34 45-46 75-80 97-102 127-138 148-168	NEK DS HL DARTAP YGRSGE GNKGAGGHSYGA ELGTDPYEDFQENWNTKHSSG
	Kolaskar & Tongaonkar	13-29 51-72 81-92 104-124	HVQLSLPVLQVRDVLVR CGLVEVEKGVLPQLEQPYVFIK HGHVMVELVAEL LGVLVPHVGEIPVAYRKVLLR
MERS-COV	**Bepipred**	8-15 22-26 50 53-56 81-84 109-116 121-123 150-154 160-162	TAQGARGT SEKHQ M ENA RHLP SSSANGSL LQG RGGYH YERDNTSCPEWMDDFEADPKGKY
	Kolaskar & Tongaonkar	26-39 56-62 66-76 85-98 103-109 131-137	QDHVSLTVPLCGSG YEVVKAM KEPLLYVPIRL GPRVYLVERLIACE VNQLAYS PYDIELV

Table 6: Intermolecular interactions of the best docked complex of nsp1-POLA1 predicted by PISA analysis

Sl.No	Amino acids of nsp1	Amino acids of POLA1	Distance (Å)	Interactions
1	Glu 2 [OE2]	Lys 923 [HZ2]	1.63	Hydrogen bond
2	Lys47 [O]	Lys 923 [HZ1]	1.82	Hydrogen bond
3	Glu 2 [OE1]	Gln 927 [HE21]	1.81	Hydrogen bond
4	Met 1 [O]	Gln 927 [HE22]	2.17	Hydrogen bond
5	Pro 115 [O]	Gln 932 [HE21]	1.78	Hydrogen bond
6	Asp 33 [OD2]	Lys 1020 [HZ1]	1.62	Hydrogen bond
7	Glu 41 [OE1]	Ans 1030 [HD21]	1.78	Hydrogen bond
8	Glu 36 [O]	Lys 1031 [HZ3]	1.80	Hydrogen bond
9	Met 1 [N]	Gln 927 [OE1]	3.50	Hydrogen bond
10	Arg 29 [HH21]	Glu 1016 [OE2]	2.11	Hydrogen bond
11	Arg 29 [HH11]	Glu 1016 [OE2]	1.94	Hydrogen bond
12	Lys47 [HZ3]	Glu 1037 [OE1]	1.63	Hydrogen bond
13	Lys47 [HZ1]	Glu 1037 [OE2]	2.36	Hydrogen bond
14	Glu 2 [OE2]	Lys 923 [NZ]	2.57	Salt bridge
15	Asp 33 [OD2]	Lys 1020 [NZ]	2.64	Salt bridge
16	Glu 37 [OE1]	Lys 1024 [NZ]	2.88	Salt bridge
17	Glu 37 [OE2]	Lys 1024 [NZ]	2.91	Salt bridge
18	Arg 29 [NH2]	Glu 1016 [OE2]	2.97	Salt bridge
19	Arg 29 [NH1]	Glu 1016 [OE2]	2.85	Salt bridge
20	Lys47 [NZ]	Glu 1037 [OE1]	2.67	Salt bridge
21	Lys47 [NZ]	Glu 1037 [OE2]	2.70	Salt bridge

Supplementary file

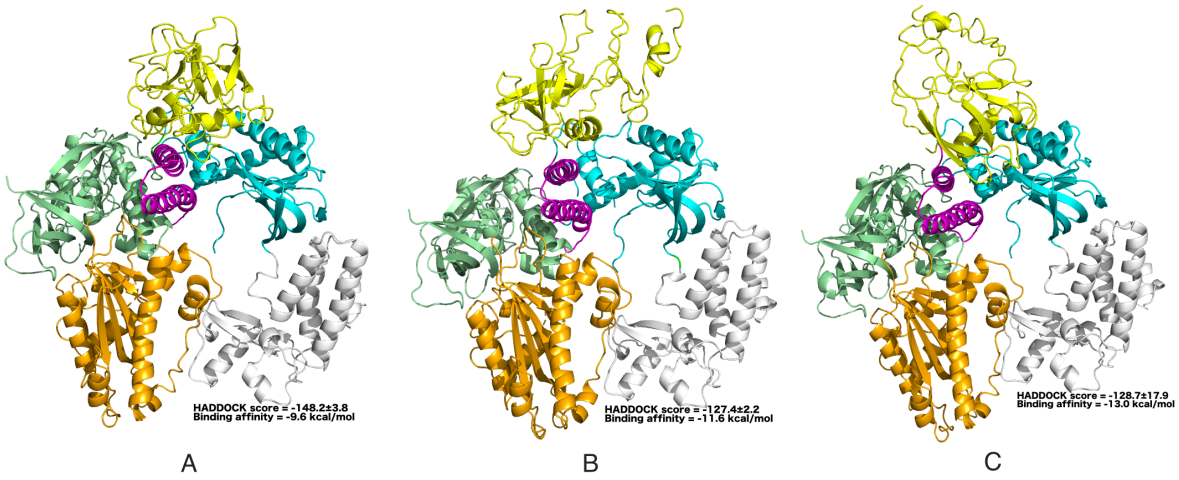

Fig. S1: Best SARS-COV2 nsp1-POLA1 complex model. A. Top model from Cluster1. B. Top model from cluster2. C. Top model from cluster5. Best model from each cluster was predicted according to lowest binding energy. Binding affinity is calculated by PRODIGY server

Table S1: Three-dimensional model validation using several analyses

Model Validation	**SARS-COV2**	**MERS-COV**
Ramachandran plot	93.95% residues in allowed region	92.07% residues in allowed region
ProSA	Z-score = -4.78	Z-score = -2.42
ProQ*	LG score = 3.578	LG score = 3.607

*Notes: LGscore > 1.5 fairly good model, LGscore > 2.5 very good model, LGscore > 4 extremely good model.

Table S2: Protein-protein docking between SARS-COV2 nsp1 and POLA1 by HADDOCK server

Total structures and total cluster number	Clus-ter(s)	Haddock score	Z-score	Cluster size	Binding energy of top selected model (kcal/mol)	Interface area of top selected model (Å²)
163 structures and 8 cluster(s)	Cluster1	-148.2±3.8	-1.5	57	-9.6	1177
	Cluster5	-128.7±17.9	-0.6	9	-13.0	1260.9
	Cluster2	-127.4±2.2	-0.6	37	-11.6	1050.0